May 11, 2023

O'Neal Comprehensive Cancer Center
University of Alabama at Birmingham
Birmingham, Alabama

Title: Accurate DCE-MRI Measurement of Glioblastoma using Point-of-care Portable Perfusion Phantom

TABLE OF CONTENTS

Harrison Kim, Ph.D., M.B.A.
University of Alabama at Birmingham
O'Neal Comprehensive Cancer Center
1670 University Blvd
Birmingham, AL 35294-3300
Tel (205-996-4088); Fax (205-975-6522)
Principal Investigator

Sub-Investigators
Mina Lobbous, MD
Kristen Riley, MD
Houman Sotoudeh, MD
Burt Nabors, MD
John, Fiveash, MD

Research Nurse Coordinator
April Riddle
Quenteeria Mooney
Sebastian Eady

National Cancer Institute
Study Supported By

UAB
Study Sponsor

Yufeng Li
Biostatistician

TABLE OF CONTENT

1.0 INTRODUCTION AND STUDY RATIONALE

Glioblastoma is the most common primary malignant type of brain tumor in adults (2). Surgical tumor resection followed by chemoradiation therapy is the standard of care for patients with glioblastoma, but its prognosis is still fairly dismal (median survival time = 15 months) (3, 4). One major concern that prevents effective treatment management is the difficulty of differentiating between pseudo-progression and true-progression (5). Pseudo-progression occurs in about 20-30% of glioblastoma patients typically within 3 months after radiotherapy with or without chemotherapy has been completed (6). Pseudo-progression is a local inflammatory reaction caused by irradiation and enhanced by concurrent chemotherapy, which leads to a transient increase of blood brain barrier (BBB) permeability (7, 8). The BBB, however, is also disrupted by neoplasm (9). Therefore, both pseudo- and true-progressions appear with an increased contrast enhancement in MRI, and there are currently no established techniques to differentiate between them (5). Pseudo-progression is typically known to be associated with better clinical outcomes (10). Thus, as illustrated in **Fig. 1**, pseudo-progression mistaken for true-progression results in the discontinuation of an effective therapy, while true-progression mistaken for pseudo-progression leads to the continuation of an ineffective therapy that may induce adverse side effects.

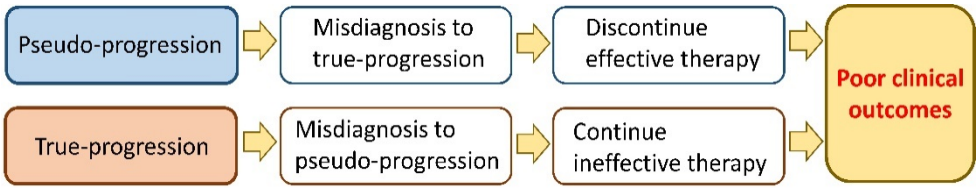

Fig. 1. Misdiagnosis of glioblastoma progression. *Pseudo-progression mistaken for true-progression results in the discontinuation of an effective therapy, while true-progression mistaken for pseudo-progression leads to the continuation of an ineffective therapy.*

Dynamic contrast enhanced magnetic resonance imaging (DCE-MRI) has the potential to differentiate between pseudo- and true-progressions in glioblastoma (11-13). The contrast-enhancing lesions of pseudo-progression are due to inflammatory BBB disruption (7, 8), whereas those of true-progression are caused by neoplastic BBB disruption (9). Therefore, true-progression typically presents higher perfusion than pseudo-progression (11-13). Dynamic susceptibility contrast (DSC) MRI is the most common technique for a non-invasive assessment of blood perfusion in the brain (14, 15). However, hemorrhagic changes within the resection cavity after surgery causes susceptibility artifacts, which often interfere with DSC-MRI, leading to false interpretation (16-18). On the other hand, DCE-MRI can assess the blood perfusion with minimal susceptibility artifacts (19-22), thus DCE-MRI may differentiate glioblastoma progression better than DSC-MRI (11).

However, the measurement variability across different MRI scanners remains a serious concern, as it hinders data comparison among institutes to retrieve a reliable threshold for accurate prognosis and subsequent treatment optimization (23). Each MRI vendor provides unique hardware configurations, pulse sequences and reconstruction algorithms, which cause variations in the quantitation of tissue contrast-agent concentration and, consequently, the DCE-MRI parameters (23). An external phantom with a known contrast-agent concentration may allow us to detect and correct the variation. Since the DCE-MRI measurement may drift due to hardware instability (24), it would be ideal if the phantom could be miniaturized to be imaged concurrently in the bore of a standard MRI scanner with a patient for real-time quality assurance.

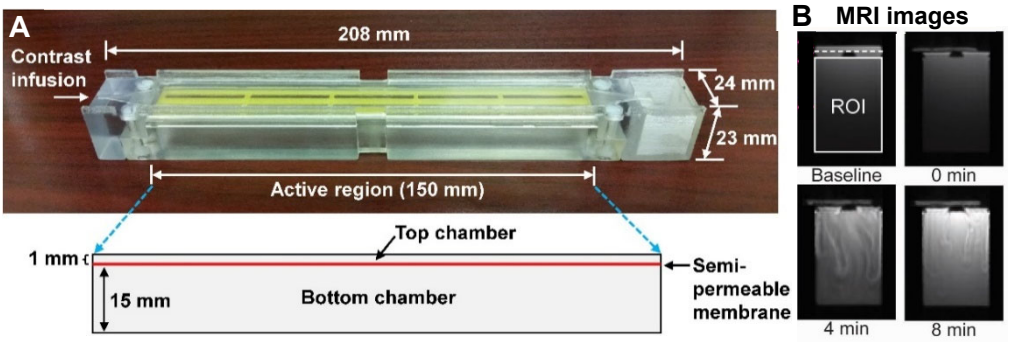

Fig. 2. Point-of-care portable perfusion phantom, P4. *(A) Photograph and schematic of the perfusion phantom. This phantom contains two chambers separated by a semi-permeable membrane. Before use, both chambers are filled with degassed/deionized water. After MRI contrast agent is infused to the top chamber (from the left), it diffuses to the bottom chamber through the semi-permeable membrane. (B) DCE-MRI images of the phantom before (baseline) and at 0, 4 and 8 minutes after MRI contrast infusion.*

The use of a static phantom comprised of multiple objects with different contrast-agent concentrations was originally suggested to correct the variation in quantitating contrast-agent concentrations of tissues (25). However, a static phantom may not serve as a reliable standard for dynamically changing tissue contrast-agent concentration, because **a)** the movement of contrast agents *in vivo* causes additional signal reduction that cannot be replicated by a static phantom, **b)** the number of data points obtained from a static phantom is small, leading to larger fitting errors, and **c)** most B_1 mapping techniques are T_1 dependent, thus the nominal flip angle delivered to a static phantom with high contrast-agent concentration cannot be accurately measured, especially in high field MRI (≥3T) (26-29). Therefore, a perfusion phantom with a varying contrast-agent concentration is required for accurate correction of MRI system-driven error. A few perfusion phantoms have been developed (30, 31), but these phantoms are too bulky to be simultaneously imaged with a human subject. In addition, these large phantoms are costly and not easily operable by typical MRI technologists, limiting the potential for widespread and routine clinical use. We recently developed a perfusion phantom named **P4** (**P**oint-of-care **P**ortable **P**erfusion **P**hantom) that significantly reduces variation in quantitating the perfusion of human tissues across different MRI scanners (1). **Figure 2A** is a photograph of the P4 with its dimensions. The P4 is composed of top and bottom chambers with a semi-permeable membrane placed between them. Both chambers are filled with degassed/deionized water before use. After starting DCE-MRI, an MRI contrast agent is infused to the top chamber at a constant rate using a syringe pump. The contrast agent displaces the water in the top chamber and diffuses to the bottom chamber as shown in **Fig. 2B**. Our lab-made software automatically segments the entire region of the bottom chamber (ROI), and the mean value within the ROI is calculated automatically, creating contrast enhancement curves (CEC) as shown in **Fig. 2C**. The dynamic change of contrast concentration in the bottom chamber was linear for 10 minutes (0.11 mM/min), when independently measured using liquid chromatography-mass spectrometry detection (LC-MS) method (32). The repeatability of phantom CEC measured by intra-class correlation coefficient (ICC) (33) was larger than 0.99 in all measurements. *Please see our paper for more details (1).* The P4 is small enough to be imaged with a human subject and is large enough not to suffer from the partial volume effect, thus MRI system-driven error can be detected during human imaging. **Before error correction, the within-subject coefficient of variation (wCV) of the volume transfer constant (K^{trans}), a DCE-MRI parameter, was about 20%, but after error correction using the P4, the**

variation was reduced to about 4% (1). Figure 3 shows the K^{trans} values averaged in each of the four organ regions of three volunteers (n=12) when two different 3T MRI scanners were used (1). Before correction, the ICC between the two data sets was 0.89, and the ICC was not improved by static phantom based error correction (ICC=0.86). *However, after P4-based error correction, ICC was increased to 0.99.* The P4 is easily operable by MRI technologists, thus it has great potential to facilitate multi-site clinical trials employing quantitative DCE-MRI (qDCE-MRI). **Of note, the clinical utility of the P4 was recently demonstrated** (34). After P4-based error correction, the change of K^{trans} in pancreatic tumors favorably responding to chemotherapy was able to be significantly differentiated from that in non-responding tumors ($p<0.0001$) (34). Besides, the P4 was able to improve the accuracy in risk stratification of prostate cancer when assessed by qDCE-MRI (35).

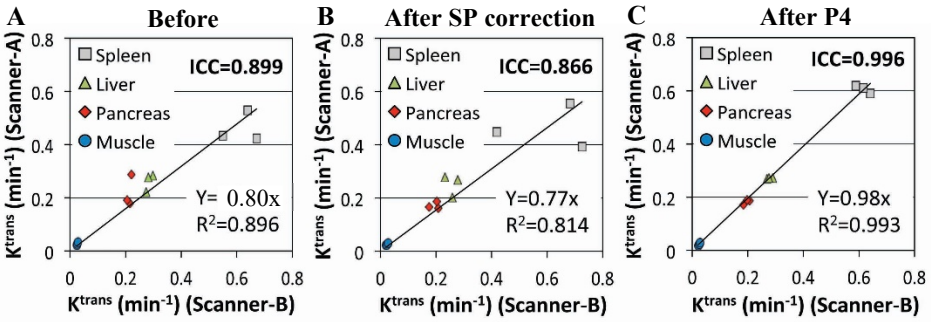

Fig. 3. K^{trans} maps before and after correction. *K^{trans} averaged in each of the four organs of three volunteers (n=12), when Scanner-A (Y-axis) or Scanner-B (X-axis) was used. (A) before or (B, C) after correction using (B) the static phantom (SP) or (C) P4 (1).*

We now hypothesize that the variability in qDCE-MRI measurement of glioblastoma across different scanners will be significantly reduced when MRI system-driven error is corrected using the P4, leading to better differentiation between pseudo- and true-progressions. **Figure 4A** shows the Gaussian distribution of the K^{trans} value of glioblastoma with true- or pseudo-progression in Yun *et al*'s study (13), where the area under the receiver operator characteristic curve (AUC) was 0.76. **Figure 4B** shows the hypothetical result when the measurement variation is reduced fivefold by our method as demonstrated in **Fig. 3**, increasing the AUC drastically (0.76 *vs* 0.99). The goal of the proposed study is to conduct the preliminary test of this hypothesis before validating our methodology in an extended multi-site clinical trial (e.g., R01 or U01 study).

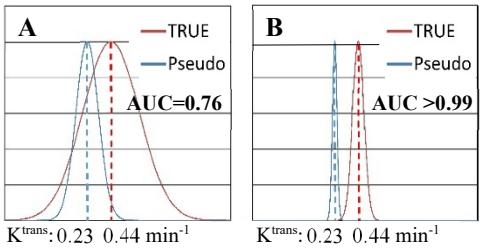

Fig. 4. *Hypothetical Gaussian distribution of glioblastoma K^{trans} values of pseudo- and true-progression groups (A) before and (B) after P4-based error correction.*

2.0 OBJECTIVES

2.1. Primary goal

To determine whether the differentiation between pseudo- and true-progressions of glioblastoma can be improved in quantitative DCE-MRI measurement when the P4 phantom is used for error correction.

2.2. Secondary goal

To determine whether the reproducibility of quantitative DCE-MRI measurement of glioblastoma can be significantly increased when MRI system-driven error is corrected using the P4 phantom.

3.0 INVESTIGATIONAL PLAN

3.1 Study Design

Figure 5 is a flow chart that illustrates our overall study plan. Each patient will be treated with surgery and followed by radiotherapy with or without chemotherapy. Then standard-of-care brain MRI will be applied every 2~3 months. If a newly or enlarged enhancing lesion is observed in one of the standard-of-care MRI and it is uncertain whether it is pseudo or true-progression, a clinical research coordinator will contact the patient for recruitment. All participants will sign an informed consent form that fully discloses the investigational nature of this study before enrollment. If the patient agrees to participate in this study, a clinical research coordinator will schedule two imaging sessions with the P4 within a one-week period, assuming that the glioblastoma perfusion parameters will not change over a week. The second imaging test will be scheduled at least 24 hours after the first one. Pseudo or true progression of glioblastoma will be determined via histopathologic analysis after biopsy (or surgery) or via the Response Assessment in Neuro-Oncology (RANO) criteria (6). In this pilot study, a total of 12 patients will be recruited. The participants will be at least 18 years old, and will not be pregnant or lactating. Subjects with safety contraindications to MRI examination and those with hemodialysis or acute/chronic renal failure will be excluded. The participants, however, will not be excluded on the basis of race, ethnicity or sex.

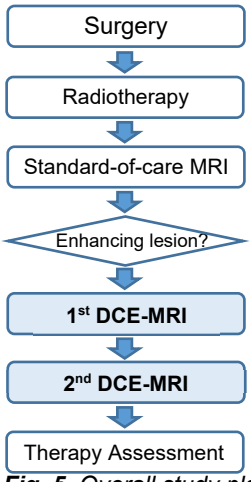

Fig. 5. *Overall study plan (TMZ=temozolomide).*

The data reproducibility across two different scanners assesses between-scanner variability combined with the inaccuracy of region of interest (ROI), arterial input function (AIF) and image co-registration. The tumor ROI will be determined by Dr. Sotoudeh (a neuro-radiologist; co-I) (see "ROI determination" section for the details). The ROIs of two scans of each subject will be matched as closely as possible to minimize intra-observer variation. We recently introduced a novel method to reliably measure individualized AIFs (36) which will be employed in this study. If the patient moves during imaging, a similarity transformation (37) will be used for 3D co-registration. The pharmacokinetic (PK) parameters (e.g., K^{trans}) within the ROI will be averaged at each scan after P4-based error correction, and the mean values of two scans will be compared to calculate the reproducibility coefficient (%RDC) using the equation, $\%RDC=2.77wCV$, where wCV is the within-subject coefficient of variation (38). The %RDC before P4-based error correction will also be calculated for comparison. Data reproducibility will be assessed using the intra-class correlation coefficient (ICC) as well. $ICC = \sigma^2_b / (\sigma^2_b + \sigma^2_w)$, where σ_b is between-subject standard deviation and σ_w is within-subject standard deviation.

Each tumor will be classified into pseudo- or true-progression based on the histopathologic data or RANO criteria. We expect approximately 40-50% of glioblastoma will be classified to

pseudo-progression, as demonstrated in previous studies (11-13). All PK parameter maps will be created within a month after image acquisition so that the image processing will not be biased by subsequent clinical findings. We will examine whether the difference of tumor PK parameters between pseudo- and true-progressions will become more statistically significant after P4-based error correction.

3.2 Primary Endpoints

The therapy response assessment based on RANO.

3.3 Study Duration

Two years.

3.4 Safety and Efficacy Monitoring

This protocol will utilize the University of Alabama at Birmingham O'Neal Comprehensive Cancer Center (CCC) Data and Safety Monitoring Plan. UAB CCC is a National Cancer Institute-designated comprehensive cancer center. Monitoring will be performed by the UAB CCC Clinical Trials Network and Monitoring Office. Serious adverse events will be reported to the chair of CCC Data Safety Monitoring Board (DSMB) within 24 hours of awareness of the event.

3.5 Therapy Modification

Two DCE-MRI imaging will be applied for each participant in addition to his/her standard-of-care. If any adverse is reported in the first DCE-MRI, the second DCE-MRI will not be applied for the participant.

3.6 Ethical Considerations

This study will be conducted in accordance with Good Clinical Practice, the Declaration of Helsinki, and 21CFRPart50 – Protection of Human Patients, Part 56 –Institutional Review Boards, and the other applicable local ethical and legal requirements. The Ethics Review Committee/Institutional Review Board (IRB) must be constituted according to Code of Federal Regulations (CFR).

3.7 Informed Consent

The principles of informed consent in the current edition of the Declaration of Helsinki will be implemented in this study. A written informed consent will be obtained in accordance with 21CFR50.25 and 21CFR50.27 before the protocol – specified procedures are carried out. Participants, their relatives, guardians or, if necessary, legal representatives must be given ample opportunity to inquire about details of the study.

3.8 Confidentiality

Participant names will not be supplied in the data. Only the participant number and initials will be recorded in the case report form (CRF). The participants will be informed that

representatives of the IRB or regulatory authorities may inspect their medical records to verify the information collected, and that all personal information made available for inspection will be handled in the strictest confidence and in accordance with local data protection laws. The investigator will maintain a personal identification list of participants (participant numbers with the corresponding names) to enable records to be identified.

4.0 SELECTION OF PARTICIPANTS

4.1 Number of Participants

We plan to accrue 12 patients at the University of Alabama at Birmingham (UAB). UAB has a total of 11 neurosurgeons for adult patients, seeing about 60 patients with recurrent glioblastoma annually. We presume that at least 16% of them will agree to participate in this study judging from our previous experience in patient enrollment.

4.2 Inclusion Criteria

Patients meeting all the following criteria will be considered for enrollment into the study.

1. Adult patients (age 18 years or older).
2. Patients with grade 3 or 4 brain tumors treated with surgery, followed by radiotherapy with or without chemotherapy.
3. Patients with a newly or enlarged enhancing lesion inside the radiation field.
4. Patients with signed informed consent.

4.3 Exclusion Criteria

Patients presenting with any of the following will not be included in the study:

1. Participants with safety contraindications to MRI examination (determined by standard clinical screening).
2. Participants on hemodialysis or with acute renal failure.
3. Participants who are pregnant, lactating or are planning to become pregnant during the study.
4. Participants who are planning to farther a child during the study.

4.4 Participants of Reproductive Potential

Participants must not be pregnant or lactating at enrollment in the study. UAB standard for screening of pregnant or lactating females is asking the participant if they are lactating, pregnant, or if there is a chance they may be pregnant. If the female answers that there is a chance that she may be pregnant, our standard is to perform an on-site urine HCG pregnancy test. The results of that test are then documented. Participants must also agree to continue to use an effective form of birth control for 6 months after taking the study. Effective birth control includes birth control pills, patch, IUD, condom, sponge, diaphragm with spermicide, or avoiding sexual activity that could cause pregnancy. If a female participant becomes pregnant during the study, she will not participate further in this study.

5.0 STUDY TREATMENTS

Each patient will undergo two DCE-MRI exams according to the timeline detailed in Fig. 5. Patients will be treated by standard-of-care therapy otherwise.

6.0 STUDY PROCEDURE AND SCHEDULE

All participants will be asked not to have caffeinated or alcohol drinks for at least 24 hours prior to imaging. The hematocrit (HCT) of each participant will be measured before imaging, which is an important factor to determine plasma input function (PIF) required for PK parameter quantification (PIF=1/(1-HCT)) (39, 40). Each subject will be instructed to put his/her head with the phantoms as shown in **Fig. 6**.

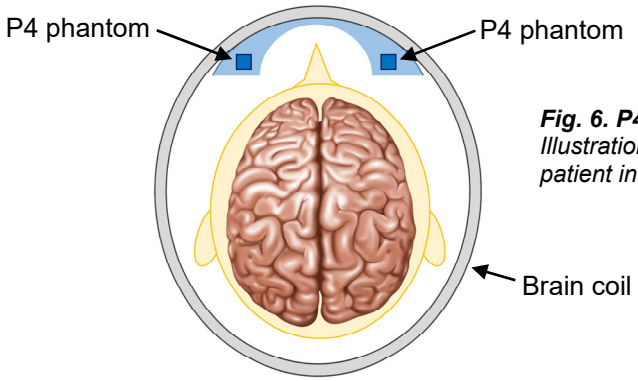

Fig. 6. P4 phantoms for brain DCE-MRI. *Illustration of the P4 phantoms located above a patient inside the brain coil.*

The phantom package will be thoroughly sanitized prior to each use. MRI scanner is equipped with a dual-channel transmit RF coil for improved B_1 field homogeneity. B_0 and B_1 shimming will be conducted, and B_1 mapping will be followed using the vendor's software (41, 42). DCE-MRI acquisition will then be carried out for 5 minutes. Gadoteridol (0.1 mmol/kg) will be injected *i.v.* to each patient at 10 s after the start of imaging procedure and will be followed by a 20-ml saline flush at a constant rate of 2 ml/s. Perfusion phantoms will be infused with 100 mM gadoteridol (0.06 ml/s; 3 ml) at 10 s after imaging start using a syringe pump (NE-1600) that is separate from the contrast agent going into the patient. Prior to DCE-MRI, T_1W images with various flip angles will be obtained for T_1 mapping (43).

7.0 SAFETY

There is minimal physical risk to undergoing the MRI test. Lying supine for 30 minutes to an hour with our phantoms located under the participant could make the participant uncomfortable. As the MRI machine obtains the images for the study, there will be loud noise. There is also a small risk that the patient may be mildly claustrophobic. When gadoteridol (MR contrast agent) is injected into the vein, a cool sensation in the arm or mild nausea is experienced by few patients. A small number of patients may have an allergic reaction to gadoteridol injected into the vein. Gadolinium based MR contrast agents can cause Nephrogenic Systemic Fibrosis (NSF) for patients with severe kidney disease. NSF appears like a bad skin disease, and it can be fatal. However, gadoteridol is known to be safe even in patients with stages 4 and 5 of chronic kidney diseases (44).

The risk of having NSF will be very low. Gadoteridol is classified as the one having the lowest risk of NSF by the European Medicines Agency (EMA) and American College of

Radiology (ACR). In animal studies, gadolinium retention has been found to be extremely low following the repeated administration of gadoteridol, and lowest in brain tissues when compared with gadolinium retention observed after repeated administration of other MR contrast agents (45-47). To our knowledge, no instances of T_1 hyperintensity in the brain have yet been observed following multiple exposure to approved doses of gadoteridol in adult or pediatric patients. In Cho et al's recent study (48), the adverse reactions of gadoteridol injection (up to a triple dose, 0.3 mmol/kg, depending upon the clinical need) were examined in a total of 6163 patients having various diseases. 8 subjects (0.13%) had mild symptoms and 2 subjects (0.03%) had modest symptoms, but not a single serious adverse event was observed. Therefore, the chance of serious adverse events following approved dose (0.1 mmol/kg) of gadoteridol is extremely low among the 12 subjects even after two dosing.

The risks of having significant claustrophobia affecting participation in this study will be low, as participants will be screened for kidney disease, claustrophobia and other conditions that would prevent them from getting an MRI. The risk of pain during insertion of an IV catheter is 100% but minimal and temporary. The risk of nausea during intravenous injection of gadoteridol is less than 1%. The risk of the patient having an allergic reaction to the MR contrast injected intravenously is less than 1%. Allergic reactions to gadoteridol typically do not require medication for reversal. If a patient is uncomfortable during a particular sequence, the exam can be terminated immediately and they will be removed from the MRI machine. During MRI test, earplugs will be given to damp loud noise. Each participant will be closely monitored via microphone while being scanned to detect any risks.

8.0 STATISTICAL METHOD

- **Sample Size Justification**

Aim 1. The K^{trans} reproducibility measured by the ICC was 0.99 in our previous experiment (1), when the P4 was used for error correction (3 volunteers x 4 tissues = 12 measurements) (see **Fig. 3C**). For brain DCE-MRI, however, the perfusion value can only be assessed in the tumor region. Thus, to achieve greater than 90% power to confirm that the data repeatability measured by the ICC is larger than 0.9 with 5% type I error, at least 12 volunteers will be needed.

Aim 2. In Yun *et al*'s study (13), the difference of tumor K^{trans} between pseudo- and true-progressions was 91% with the standard deviation (SD) of approximately 50% in each group (p=0.004). If the mean and SD of each group in the proposed study will be the same with those of Yun *et al*'s study (0.44±0.25 *vs* 0.23±0.10 min^{-1}), the sample size (n=12) will have 55% power at a 5% significant level to differentiate the two groups (assuming n=6 per group) using a one-side two-group student t-test. However, if the SD is reduced to ≤35% using the P4, the power will be increased to ≥90%.

- **Statistical Analysis**

Descriptive analysis with the mean and SD will be presented for each experimental parameter and each time point. Graphic presentation will be considered when appropriate. Due to repeated measurement, ANOVA analysis with a mixed model will be used to estimate the measurement error (within error) with two-sided 95% confidence interval (49). Data

reproducibility will be assessed using both the ICC and %RDC (33). Tumor PK parameters between pseudo- and true-progressions will be compared using two-group student t-test (50). Data will be transformed using natural logarithms if the variability is found to be dependent upon its mean value. All data will be analyzed using SAS (SAS institute, Cary, NC) by Dr. Li (see her support letter).

9.0 CLOSURE OF THE STUDY

The study will be closed at the site upon completion.

10.0 REFERENCES

1. Kim H, Mousa M, Schexnailder P, Hergenrother R, Bolding M, Ntsikoussalabongui B, Thomas V, Morgan DE. Portable perfusion phantom for quantitative DCE-MRI of the abdomen. Med Phys. 2017. doi: 10.1002/mp.12466. PubMed PMID: 28692137. Available from: https://www.ncbi.nlm.nih.gov/pubmed/28692137.
2. Cancer Facts & Figures 2019. American Cancer Society
3. Erpolat OP, Akmansu M, Goksel F, Bora H, Yaman E, Buyukberber S. Outcome of newly diagnosed glioblastoma patients treated by radiotherapy plus concomitant and adjuvant temozolomide: a long-term analysis. Tumori. 2009;95(2):191-7. Epub 2009/07/08. PubMed PMID: 19579865. Available from: https://www.ncbi.nlm.nih.gov/pubmed/19579865.
4. Jeon HJ, Kong DS, Park KB, Lee JI, Park K, Kim JH, Kim ST, Lim DH, Kim WS, Nam DH. Clinical outcome of concomitant chemoradiotherapy followed by adjuvant temozolomide therapy for glioblastaomas: single-center experience. Clin Neurol Neurosurg. 2009;111(8):679-82. Epub 2009/07/31. doi: 10.1016/j.clineuro.2009.06.013. PubMed PMID: 19640635. Available from: https://www.ncbi.nlm.nih.gov/pubmed/19640635.
5. Johnson DR, Guerin JB, Ruff MW, Fang S, Hunt CH, Morris JM, Pearse Morris P, Kaufmann TJ. Glioma response assessment: Classic pitfalls, novel confounders, and emerging imaging tools. Br J Radiol. 2018:20180730. Epub 2018/11/10. doi: 10.1259/bjr.20180730. PubMed PMID: 30412421. Available from: https://www.ncbi.nlm.nih.gov/pubmed/30412421.
6. Wen PY, Macdonald DR, Reardon DA, Cloughesy TF, Sorensen AG, Galanis E, Degroot J, Wick W, Gilbert MR, Lassman AB, Tsien C, Mikkelsen T, Wong ET, Chamberlain MC, Stupp R, Lamborn KR, Vogelbaum MA, van den Bent MJ, Chang SM. Updated response assessment criteria for high-grade gliomas: response assessment in neuro-oncology working group. J Clin Oncol. 2010;28(11):1963-72. Epub 2010/03/17. doi: 10.1200/JCO.2009.26.3541. PubMed PMID: 20231676. Available from: https://www.ncbi.nlm.nih.gov/pubmed/20231676.
7. Brandsma D, Stalpers L, Taal W, Sminia P, van den Bent MJ. Clinical features, mechanisms, and management of pseudoprogression in malignant gliomas. Lancet Oncol. 2008;9(5):453-61. Epub 2008/05/03. doi: 10.1016/S1470-2045(08)70125-6. PubMed PMID: 18452856. Available from: https://www.ncbi.nlm.nih.gov/pubmed/18452856.
8. Gerstner ER, McNamara MB, Norden AD, Lafrankie D, Wen PY. Effect of adding temozolomide to radiation therapy on the incidence of pseudo-progression. J Neurooncol. 2009;94(1):97-101. Epub 2009/02/18. doi: 10.1007/s11060-009-9809-4. PubMed PMID: 19221865. Available from: https://www.ncbi.nlm.nih.gov/pubmed/19221865.
9. Schneider SW, Ludwig T, Tatenhorst L, Braune S, Oberleithner H, Senner V, Paulus W. Glioblastoma cells release factors that disrupt blood-brain barrier features. Acta Neuropathol.

2004;107(3):272-6. Epub 2004/01/20. doi: 10.1007/s00401-003-0810-2. PubMed PMID: 14730455. Available from: https://www.ncbi.nlm.nih.gov/pubmed/14730455.
10. Clarke JL, Chang S. Pseudoprogression and pseudoresponse: challenges in brain tumor imaging. Curr Neurol Neurosci Rep. 2009;9(3):241-6. Epub 2009/04/08. PubMed PMID: 19348713. Available from: https://www.ncbi.nlm.nih.gov/pubmed/19348713.
11. Shin KE, Ahn KJ, Choi HS, Jung SL, Kim BS, Jeon SS, Hong YG. DCE and DSC MR perfusion imaging in the differentiation of recurrent tumour from treatment-related changes in patients with glioma. Clin Radiol. 2014;69(6):e264-72. Epub 2014/03/07. doi: 10.1016/j.crad.2014.01.016. PubMed PMID: 24594379. Available from: https://www.ncbi.nlm.nih.gov/pubmed/24594379.
12. Thomas AA, Arevalo-Perez J, Kaley T, Lyo J, Peck KK, Shi W, Zhang Z, Young RJ. Dynamic contrast enhanced T1 MRI perfusion differentiates pseudoprogression from recurrent glioblastoma. J Neurooncol. 2015;125(1):183-90. Epub 2015/08/16. doi: 10.1007/s11060-015-1893-z. PubMed PMID: 26275367; PMCID: PMC4726629. Available from: https://www.ncbi.nlm.nih.gov/pubmed/26275367.
13. Yun TJ, Park CK, Kim TM, Lee SH, Kim JH, Sohn CH, Park SH, Kim IH, Choi SH. Glioblastoma treated with concurrent radiation therapy and temozolomide chemotherapy: differentiation of true progression from pseudoprogression with quantitative dynamic contrast-enhanced MR imaging. Radiology. 2015;274(3):830-40. Epub 2014/10/22. doi: 10.1148/radiol.14132632. PubMed PMID: 25333475. Available from: https://www.ncbi.nlm.nih.gov/pubmed/25333475.
14. Boxerman JL, Shiroishi MS, Ellingson BM, Pope WB. Dynamic Susceptibility Contrast MR Imaging in Glioma: Review of Current Clinical Practice. Magn Reson Imaging Clin N Am. 2016;24(4):649-70. Epub 2016/10/16. doi: 10.1016/j.mric.2016.06.005. PubMed PMID: 27742108. Available from: https://www.ncbi.nlm.nih.gov/pubmed/27742108.
15. Delgado AF, Delgado AF. Discrimination between Glioma Grades II and III Using Dynamic Susceptibility Perfusion MRI: A Meta-Analysis. AJNR Am J Neuroradiol. 2017;38(7):1348-55. Epub 2017/05/20. doi: 10.3174/ajnr.A5218. PubMed PMID: 28522666. Available from: https://www.ncbi.nlm.nih.gov/pubmed/28522666.
16. Aronen HJ, Perkio J. Dynamic susceptibility contrast MRI of gliomas. Neuroimaging Clin N Am. 2002;12(4):501-23. Epub 2003/04/12. PubMed PMID: 12687908. Available from: https://www.ncbi.nlm.nih.gov/pubmed/12687908.
17. Grandin CB. Assessment of brain perfusion with MRI: methodology and application to acute stroke. Neuroradiology. 2003;45(11):755-66. Epub 2003/10/15. doi: 10.1007/s00234-003-1024-y. PubMed PMID: 14557902. Available from: https://www.ncbi.nlm.nih.gov/pubmed/14557902.
18. Speck O, Chang L, DeSilva NM, Ernst T. Perfusion MRI of the human brain with dynamic susceptibility contrast: gradient-echo versus spin-echo techniques. J Magn Reson Imaging. 2000;12(3):381-7. Epub 2000/09/19. PubMed PMID: 10992304. Available from: https://www.ncbi.nlm.nih.gov/pubmed/10992304.
19. Barnes SL, Whisenant JG, Loveless ME, Yankeelov TE. Practical dynamic contrast enhanced MRI in small animal models of cancer: data acquisition, data analysis, and interpretation. Pharmaceutics. 2012;4(3):442-78. Epub 2012/10/30. doi: 10.3390/pharmaceutics4030442. PubMed PMID: 23105959; PMCID: 3480221. Available from: http://www.ncbi.nlm.nih.gov/pubmed/23105959.

20. Zhang CC, Yan Z, Giddabasappa A, Lappin PB, Painter CL, Zhang Q, Li G, Goodman J, Simmons B, Pascual B, Lee J, Levkoff T, Nichols T, Xie Z. Comparison of dynamic contrast-enhanced MR, ultrasound and optical imaging modalities to evaluate the antiangiogenic effect of PF-03084014 and sunitinib. Cancer medicine. 2014;3(3):462-71. Epub 2014/02/28. doi: 10.1002/cam4.215. PubMed PMID: 24573979; PMCID: 4101737. Available from: http://www.ncbi.nlm.nih.gov/pubmed/24573979.
21. Craciunescu OI, Blackwell KL, Jones EL, Macfall JR, Yu D, Vujaskovic Z, Wong TZ, Liotcheva V, Rosen EL, Prosnitz LR, Samulski TV, Dewhirst MW. DCE-MRI parameters have potential to predict response of locally advanced breast cancer patients to neoadjuvant chemotherapy and hyperthermia: a pilot study. Int J Hyperthermia. 2009;25(6):405-15. Epub 2009/08/07. doi: 10.1080/02656730903022700. PubMed PMID: 19657852; PMCID: 2783501. Available from: http://www.ncbi.nlm.nih.gov/pubmed/19657852.
22. Kim H, Folks KD, Guo L, Sellers JC, Fineberg NS, Stockard CR, Grizzle WE, Buchsbaum DJ, Morgan DE, George JF, Zinn KR. Early therapy evaluation of combined cetuximab and irinotecan in orthotopic pancreatic tumor xenografts by dynamic contrast-enhanced magnetic resonance imaging. Mol Imaging. 2011;10(3):153-67. Epub 2011/04/19. PubMed PMID: 21496446. Available from: http://www.ncbi.nlm.nih.gov/entrez/query.fcgi?cmd=Retrieve&db=PubMed&dopt=Citation&list_uids=21496446.
23. Kim H. Variability in Quantitative DCE-MRI: Sources and Solutions. J Nat Sci. 2018;4(1). Epub 2018/03/13. PubMed PMID: 29527572; PMCID: PMC5841165. Available from: https://www.ncbi.nlm.nih.gov/pubmed/29527572.
24. O'Callaghan J, Wells J, Richardson S, Holmes H, Yu Y, Walker-Samuel S, Siow B, Lythgoe MF. Is your system calibrated? MRI gradient system calibration for pre-clinical, high-resolution imaging. PLoS One. 2014;9(5):e96568. doi: 10.1371/journal.pone.0096568. PubMed PMID: 24804737; PMCID: PMC4013024. Available from: https://www.ncbi.nlm.nih.gov/pubmed/24804737.
25. Jackson EF, Gupta SN, A. RM, Ashton EA, Karczmar GS, Evelhoch JL, Buonocore MH, Purdy DE, Zahlmann G. QIBA DCE-MRI technical committee update: phantom studies and first DCEMRI profile. Proceedings of the 96th Scientific Assembly and Annual Meeting of the Radiological Society of North America, Chicago, Ill, USA, December 2010. 2010.
26. Cunningham CH, Pauly JM, Nayak KS. Saturated double-angle method for rapid B1+ mapping. Magnetic resonance in medicine. 2006;55(6):1326-33. Epub 2006/05/10. doi: 10.1002/mrm.20896. PubMed PMID: 16683260. Available from: http://www.ncbi.nlm.nih.gov/pubmed/16683260.
27. Choi N, Lee J, Kim MO, Shin J, Kim DH. A modified multi-echo AFI for simultaneous B1(+) magnitude and phase mapping. Magnetic resonance imaging. 2014;32(4):314-20. Epub 2014/02/12. doi: 10.1016/j.mri.2013.12.005. PubMed PMID: 24512801. Available from: http://www.ncbi.nlm.nih.gov/pubmed/24512801.
28. Morrell GR. A phase-sensitive method of flip angle mapping. Magnetic resonance in medicine. 2008;60(4):889-94. Epub 2008/09/26. doi: 10.1002/mrm.21729. PubMed PMID: 18816809. Available from: http://www.ncbi.nlm.nih.gov/pubmed/18816809.
29. Jiru F, Klose U. Fast 3D radiofrequency field mapping using echo-planar imaging. Magnetic resonance in medicine. 2006;56(6):1375-9. Epub 2006/11/08. doi: 10.1002/mrm.21083. PubMed PMID: 17089359. Available from: http://www.ncbi.nlm.nih.gov/pubmed/17089359.

30. Knight SP, Browne JE, Meaney JF, Smith DS, Fagan AJ. A novel anthropomorphic flow phantom for the quantitative evaluation of prostate DCE-MRI acquisition techniques. Physics in Medicine and Biology. 2016;61:7466-83.
31. Freed M, de Zwart JA, Hariharan P, Myers MR, Badano A. Development and characterization of a dynamic lesion phantom for the quantitative evaluation of dynamic contrast-enhanced MRI. Medical physics. 2011;38(10):5601-11. Epub 2011/10/14. doi: 10.1118/1.3633911. PubMed PMID: 21992378; PMCID: 3195376. Available from: http://www.ncbi.nlm.nih.gov/pubmed/21992378.
32. Jia J, Keiser M, Nassif A, Siegmund W, Oswald S. A LC-MS/MS method to evaluate the hepatic uptake of the liver-specific magnetic resonance imaging contrast agent gadoxetate (Gd-EOB-DTPA) in vitro and in humans. J Chromatogr B Analyt Technol Biomed Life Sci. 2012;891-892:20-6. doi: 10.1016/j.jchromb.2012.02.014. PubMed PMID: 22391331. Available from: https://www.ncbi.nlm.nih.gov/pubmed/22391331.
33. Bartlett JW, Frost C. Reliability, repeatability and reproducibility: analysis of measurement errors in continuous variables. Ultrasound in obstetrics & gynecology : the official journal of the International Society of Ultrasound in Obstetrics and Gynecology. 2008;31(4):466-75. Epub 2008/02/29. doi: 10.1002/uog.5256. PubMed PMID: 18306169. Available from: http://www.ncbi.nlm.nih.gov/pubmed/18306169.
34. Kim H, Morgan DE, Schexnailder P, Navari RM, Willams GR, Rose JB, Li Y, Paluri R. Accurate Therapeutic Response Assessment of Pancreatic Ductal Adenocarcinoma using Quantitative DCE-MRI with a Point-of-Care Perfusion Phantom: A Pilot Study. Invest Radiol. 2018 [Epub ahead of print].
35. Kim H, Thomas JV, Nix JW, Gordetsky JB, Li Y, Rais-Bahrami S. Portable Perfusion Phantom Offers Quantitative Dynamic Contrast-Enhanced Magnetic Resonance Imaging for Accurate Prostate Cancer Grade Stratification: A Pilot Study. Acad Radiol. 2021;28(3):405-13. Epub 2020/04/01. doi: 10.1016/j.acra.2020.02.027. PubMed PMID: 32224036; PMCID: PMC7529802. Available from: https://www.ncbi.nlm.nih.gov/pubmed/32224036.
36. Kim H. Modification of population based arterial input function to incorporate individual variation. Magn Reson Imaging. 2017. Epub 2017/09/30. doi: 10.1016/j.mri.2017.09.010. PubMed PMID: 28958876. Available from: https://www.ncbi.nlm.nih.gov/pubmed/28958876.
37. Arfken G. Mathematical Methods for Physicists, 3rd ed.1985.
38. Raunig DL, McShane LM, Pennello G, Gatsonis C, Carson PL, Voyvodic JT, Wahl RL, Kurland BF, Schwarz AJ, Gonen M, Zahlmann G, Kondratovich MV, O'Donnell K, Petrick N, Cole PE, Garra B, Sullivan DC, Group QTPW. Quantitative imaging biomarkers: a review of statistical methods for technical performance assessment. Stat Methods Med Res. 2015;24(1):27-67. Epub 2014/06/13. doi: 10.1177/0962280214537344. PubMed PMID: 24919831; PMCID: PMC5574197. Available from: https://www.ncbi.nlm.nih.gov/pubmed/24919831.
39. Tofts PS, Brix G, Buckley DL, Evelhoch JL, Henderson E, Knopp MV, Larsson HB, Lee TY, Mayr NA, Parker GJ, Port RE, Taylor J, Weisskoff RM. Estimating kinetic parameters from dynamic contrast-enhanced T(1)-weighted MRI of a diffusable tracer: standardized quantities and symbols. J Magn Reson Imaging. 1999;10(3):223-32. Epub 1999/10/03. doi: 10.1002/(SICI)1522-2586(199909)10:3<223::AID-JMRI2>3.0.CO;2-S [pii]. PubMed PMID: 10508281. Available from: http://www.ncbi.nlm.nih.gov/entrez/query.fcgi?cmd=Retrieve&db=PubMed&dopt=Citation&list_uids=10508281.

40. Tofts PS. Modeling tracer kinetics in dynamic Gd-DTPA MR imaging. Journal of magnetic resonance imaging : JMRI. 1997;7(1):91-101. Epub 1997/01/01. PubMed PMID: 9039598. Available from: http://www.ncbi.nlm.nih.gov/pubmed/9039598.
41. Chung S, Kim D, Breton E, Axel L. Rapid B1+ mapping using a preconditioning RF pulse with TurboFLASH readout. Magnetic resonance in medicine. 2010;64(2):439-46. Epub 2010/07/29. doi: 10.1002/mrm.22423. PubMed PMID: 20665788; PMCID: 2929762. Available from: http://www.ncbi.nlm.nih.gov/pubmed/20665788.
42. Sacolick LI, Wiesinger F, Hancu I, Vogel MW. B1 mapping by Bloch-Siegert shift. Magnetic resonance in medicine. 2010;63(5):1315-22. Epub 2010/05/01. doi: 10.1002/mrm.22357. PubMed PMID: 20432302; PMCID: 2933656. Available from: http://www.ncbi.nlm.nih.gov/pubmed/20432302.
43. Liberman G, Louzoun Y, Ben Bashat D. T(1) mapping using variable flip angle SPGR data with flip angle correction. J Magn Reson Imaging. 2014;40(1):171-80. doi: 10.1002/jmri.24373. PubMed PMID: 24990618. Available from: https://www.ncbi.nlm.nih.gov/pubmed/24990618.
44. Woolen SA, Shankar PR, Gagnier JJ, MacEachern MP, Singer L, Davenport MS. Risk of Nephrogenic Systemic Fibrosis in Patients With Stage 4 or 5 Chronic Kidney Disease Receiving a Group II Gadolinium-Based Contrast Agent: A Systematic Review and Meta-analysis. JAMA Intern Med. 2020;180(2):223-30. doi: 10.1001/jamainternmed.2019.5284. PubMed PMID: 31816007; PMCID: PMC6902198. Available from: https://www.ncbi.nlm.nih.gov/pubmed/31816007.
45. Bussi S, Coppo A, Botteron C, Fraimbault V, Fanizzi A, De Laurentiis E, Colombo Serra S, Kirchin MA, Tedoldi F, Maisano F. Differences in gadolinium retention after repeated injections of macrocyclic MR contrast agents to rats. J Magn Reson Imaging. 2018;47(3):746-52. Epub 2017/07/22. doi: 10.1002/jmri.25822. PubMed PMID: 28730643; PMCID: PMC5836870. Available from: https://www.ncbi.nlm.nih.gov/pubmed/28730643.
46. Jost G, Frenzel T, Boyken J, Lohrke J, Nischwitz V, Pietsch H. Long-term Excretion of Gadolinium-based Contrast Agents: Linear versus Macrocyclic Agents in an Experimental Rat Model. Radiology. 2019;290(2):340-8. Epub 2018/11/14. doi: 10.1148/radiol.2018180135. PubMed PMID: 30422091. Available from: https://www.ncbi.nlm.nih.gov/pubmed/30422091.
47. McDonald RJ, McDonald JS, Dai D, Schroeder D, Jentoft ME, Murray DL, Kadirvel R, Eckel LJ, Kallmes DF. Comparison of Gadolinium Concentrations within Multiple Rat Organs after Intravenous Administration of Linear versus Macrocyclic Gadolinium Chelates. Radiology. 2017;285(2):536-45. Epub 2017/06/24. doi: 10.1148/radiol.2017161594. PubMed PMID: 28640692. Available from: https://www.ncbi.nlm.nih.gov/pubmed/28640692.
48. Cho SB, Lee AL, Chang HW, Kim KA, Yoo WJ, Yeom JA, Rho MH, Kim SJ, Lim YJ, Han M. Prospective Multicenter Study of the Safety of Gadoteridol in 6163 Patients. J Magn Reson Imaging. 2020;51(3):861-8. Epub 2019/10/31. doi: 10.1002/jmri.26940. PubMed PMID: 31663202; PMCID: PMC7027821. Available from: https://www.ncbi.nlm.nih.gov/pubmed/31663202.
49. Bland JM, Altman DG. Measurement error. BMJ. 1996;313(7059):744. Epub 1996/09/21. PubMed PMID: 8819450; PMCID: PMC2352101. Available from: https://www.ncbi.nlm.nih.gov/pubmed/8819450.
50. Neter J, Kutner MH, Nachtsheim JC, Wasserman W. Applied linear statistical models. Fourth ed. Columbus: The McGraw-Hill Companies, Inc.; 1996.